Nicotinamide N-methyltransferase sustains a core epigenetic program that promotes metastatic colonization in breast cancer

Appendix Figures

Table of contents - Appendix Figures

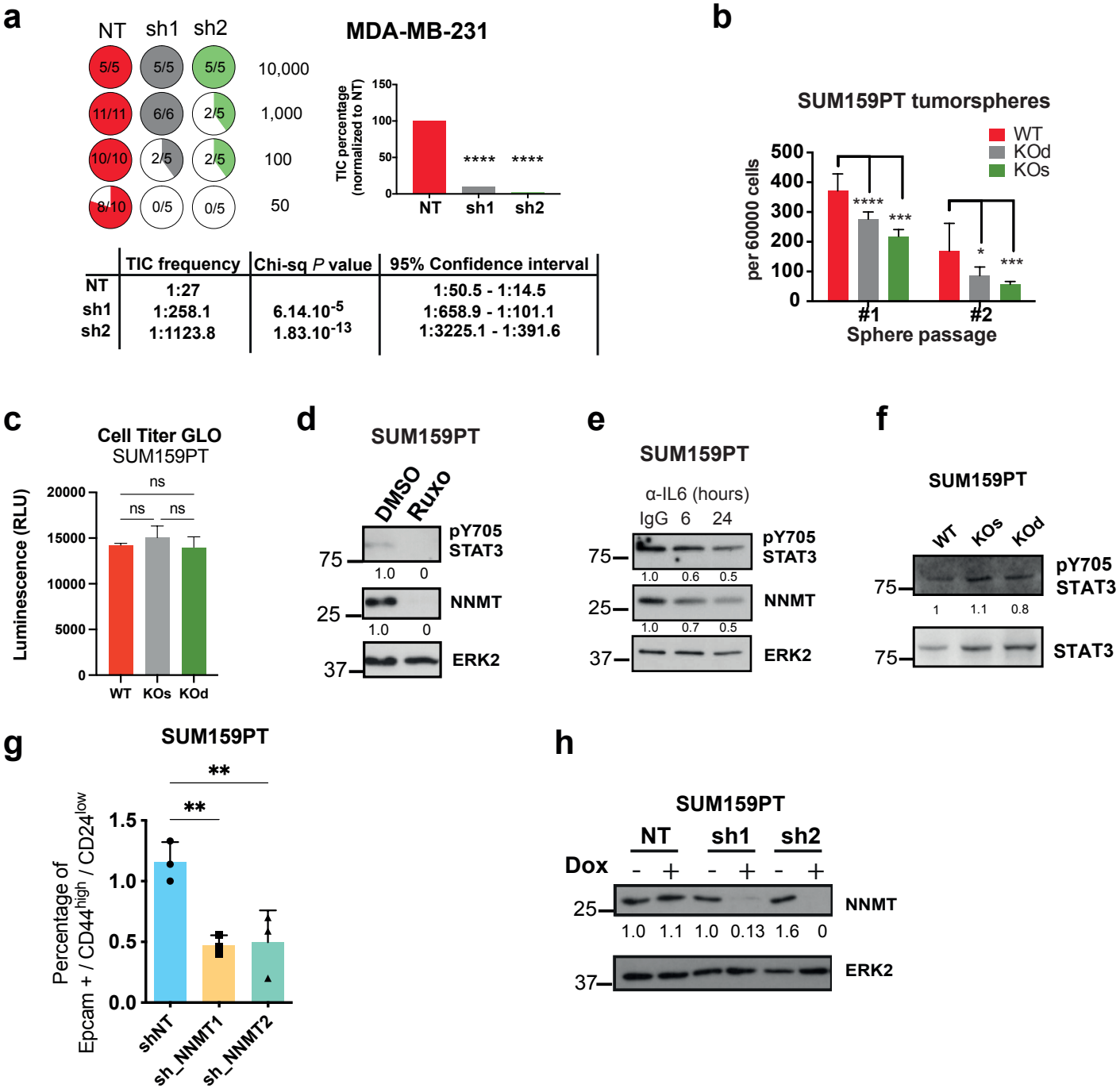

Appendix Figure S1. NNMT enhances tumor initiating capacity and stem features.

a. Quantification of tumor incidence (pie charts) following orthotopic injection into NSG mice of MDA-MB-231 cells transfected with lentiviral vectors encoding sh NT (non-targeting), sh NNMT_1 and sh NNMT_2. ****P < 0.0001; Mann-Whitney test.

b. Bar plots showing primary (#1) and secondary (#2) tumorsphere numbers derived from SUM159PT WT, NNMT KOs and NNMT KOd cells NNMT. n = 9 data points, 3 biological replicates, each with 3 technical replicates. *P < 0.05, **P < 0.01, ***P < 0.001; Mann-Whitney test. All data are mean ± SD.

c. Bar graph representing Cell-Titer GLO assay quantification from SUM159PT WT, KOs NNMT and KOd NNMT cells. n = 6 experimental replicates. n.s., non-signifcant; One-way ANOVA. All data are means ± SD.

d. Immunoblots showing the abundance of phospho-STAT3 Y705 and NNMT in SUM159PT treated with DMSO or JAK inhibitor Ruxolinitb. ERK2 was used as loading control.

e. Immunoblots showing the abundance of phospho-STAT3 Y705 and NNMT in SUM159PT treated with monoclonal IgG or anti-IL6 blocking antibodies (2.5 ug/ml, for 6h and 24h) in secondary tumor spheres. ERK2 was used as loading control.

f. Immunoblots showing the abundance of phospho-STAT3 Y705 and STAT3 in SUM159PT WT, KOS and KOD.

g. Bar plot quantification of Epcam (+), CD44 (high), and CD24 (low) SUM159PT cells by FACS, at day 6 of doxycycline- inducible knockdown of NNMT using two independent sh RNAs. n = 3 biological replicates. **P < 0.01; One-way ANOVA. Data are mean ± SD.

h. Immunoblots showing the abundance of NNMT in SUM159PT transfected with lentiviral doxycycline-inducible expression vectors encoding non-targeting or NNMT-targeting sh RNAs. ERK2 was used as loading control.

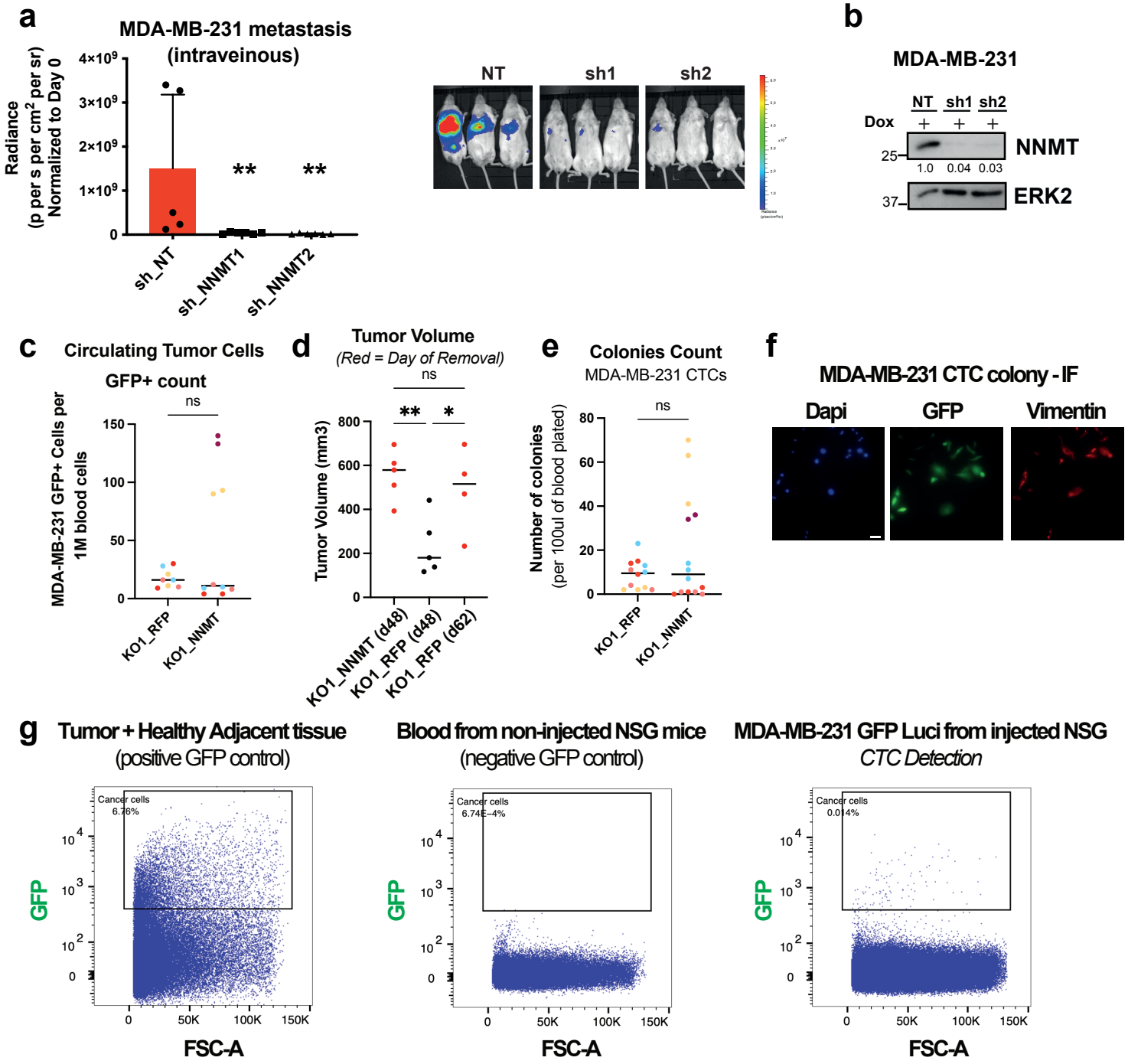

Appendix Figure S2. NNMT, metastasis and circulating tumor cells (CTC) shedding.

a. Bar graph quantification and representative bioluminescence imaging of metastases at day 41 after injection of 100 000 MDA-MB-231 sh NT (non-targeting), sh NNMT_1 and sh NNMT_2 cells intravenously. Mice were fed with doxycycline food to sustain shRNA expression during the whole experiment. Representative images are shown. n = 5 to 6 animals per group. *P < 0.05, **P < 0.01, ***P < 0.001; Mann-Whitney test. All data are mean ± SD.

b. Immunoblots showing the abundance of NNMT in MDA-MB-231 transfected with lentiviral doxycycline-inducible expression vectors encoding non-targeting or NNMT-targeting sh RNAs. ERK2 was used as loading control.

c. Dot plot showing FACS quantification of GFP-positive circulating tumor cells (CTCs) analyzed from the blood of NSG mice, orthotopically injected with MDA-MB-231 KO1_RFP or KO1_NNMT breast cancer cells. n = 4 to 5 animals per group, with 2 technical replicates. Mann-Whitney test.

d. Dot plot showing primary tumors volume measurement of MDA-MB-231 KO1_RFP or KO1_NNMT, at day 48 (removal of KO1_NNMT tumors) and at day 62 (removal of KO1_RFP tumors). Red dots indicated day of removal for the respective experimental conditions. At the day of removal, no significant difference between KO1_RFP or KO1_NNMT primary tumors was observed. n = 4 to 5 animals per group. One-way ANOVA.

e. Dot plot showing quantification of circulating tumor cells (CTCs) derived colonies, after plating of 100ul of blood collected from MDA-MB-231 KO1_RFP or KO1_NNMT orthotopically injected NSG mice, in 10% FCS DMEM for 7 days. n = 4 to 5 animals per group, with 2 to 3 technical replicates. n.s: non-significant; Mann-Whitney test.

f. Representative images of immunostaining of CTC colonies grown for 8 days using Dapi, GFP and Vimentin, confirming the identify of MDA-MB-231 cells. 100 ul of blood was plated in DMEM using a 6-well plate format. Scale bar: 10 uM.

g. Representative images FACS plot showing CTC detection using GFP fluorescence, in comparison to positive control (Tumor + Healthy adjacent tissue) and negative control (blood from non-injected mice).

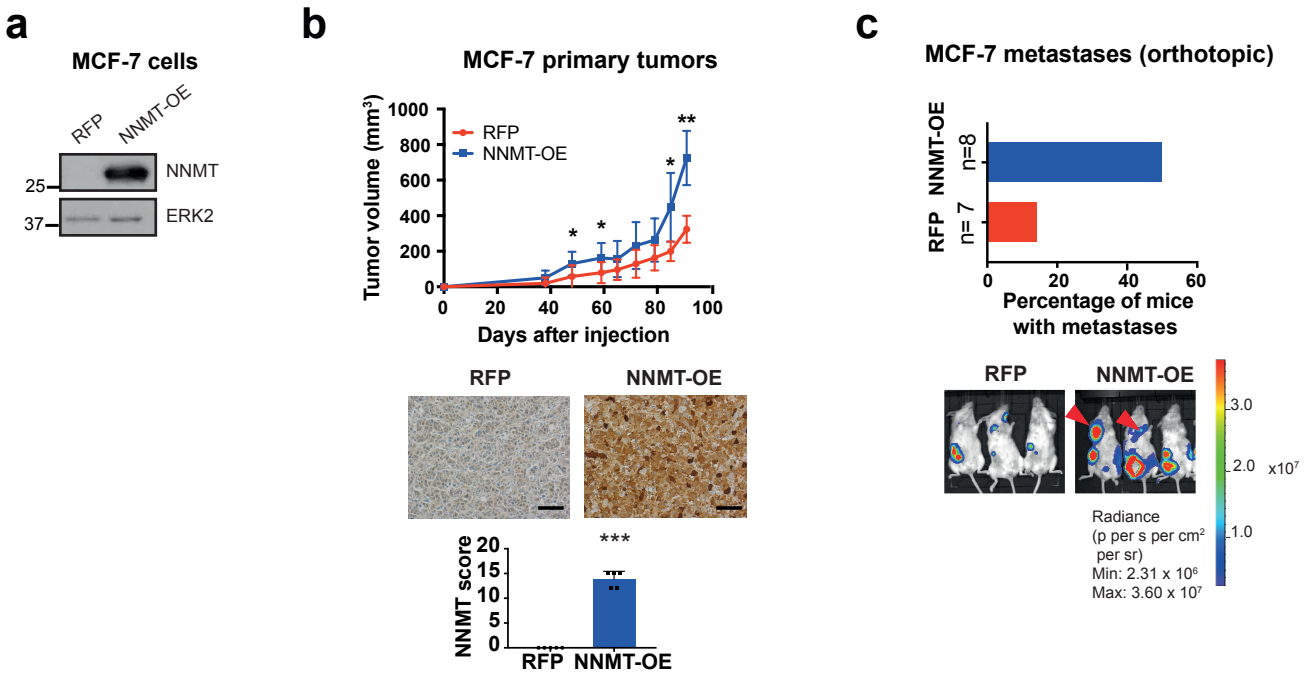

Appendix Figure S3. Expression of NNMT in luminal breast cancer cell line promotes tumor growth and metastasis.

a, Immunoblot showing levels of NNMT and ERK2 (loading control) in MCF-7 cells infected with a lentiviral RFP control vector or the full NNMT ORF sequence.

b, Upper panel: Kinetics of primary tumor growth of MCF-7_RFP (n = 8 mice) and NNMT-overexpressing (OE) (n = 11 mice) sublines upon orthotopic injection of 100 000 cells. Lower panel: representative images of NNMT immunostaining in the primary tumors and respective quantification. *P < 0.05, **P < 0.01, ***P < 0.001; Mann-Whitney U-test. Data are means ± SD. Scale bar: 100 µm.

c, Upper panel: Bar graph quantification of the incidence of lymph node metastases in MCF-7_RFP and NNMT-overexpressing (OE) cells; Lower panel: representative bioluminescence images of metastases formed after removal of the primary tumor from MCF-7_RFP or NNMT-OE cells. Arrows indicate lymph node metastases.

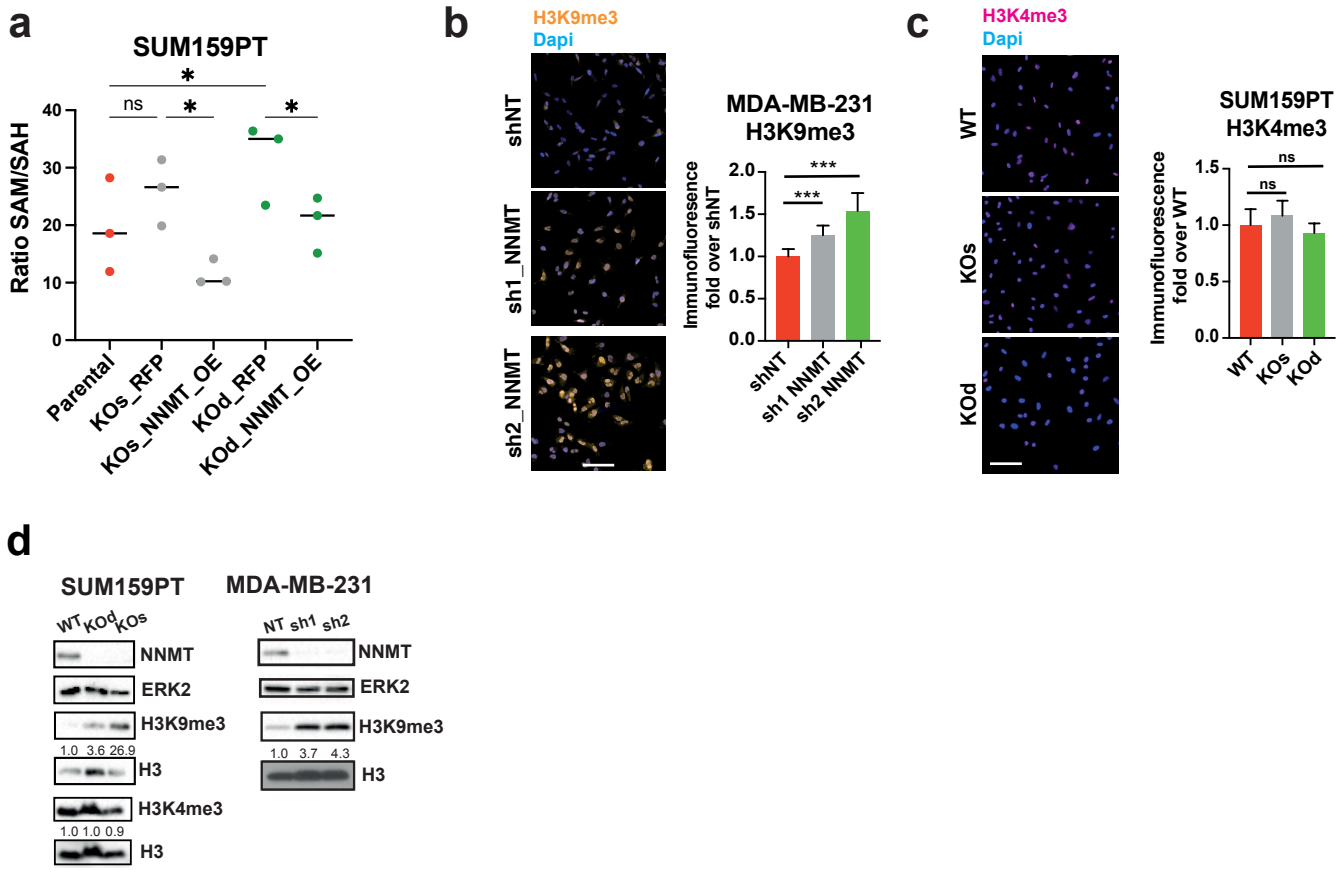

Appendix Figure S4. NNMT depletion increases SAM and H3K9me3 abundance.

a, Bar graph depicting ratio of S-adenosylmethionine (SAM): S-adenosylhomocysteine (SAH) in SUM159PT WT, KOd_RFP, KOd_NNMT_OE (rescue NNMT), KOs_RFP and KOs_NNMT_OE (rescue NNMT), profiled by mass-spectrometry. *P < 0.05; One-way ANOVA.

b, Bar graph and images depicting H3K9me3 signal by immunofluorescence in MDA-MB-231 sh NT, sh1 NNMT, and sh2 NNMT cells. n = 3 experimental replicates with 4 technical replicates each. ***P < 0.001; Kruskal-Wallis test. All data are means ± SD. Scale bar: 50 μm.

c, Bar graph and images depicting H3K4me3 signal by immunofluorescence in SUM159PT WT, KOs, and KOd cells. n = 3 to 4 experimental replicates with 4 to 5 technical replicates each. n.s., not significant; Kruskal-Wallis test. All data are means ± SD. Scale bar: 50 μm.

d, Immunoblots showing upregulation of H3K9me3 in NNMT KO cells. ERK2 was used as a loading control for NNMT levels. H3 was used as loading control for H3K9me3 and H3K4me3 levels.

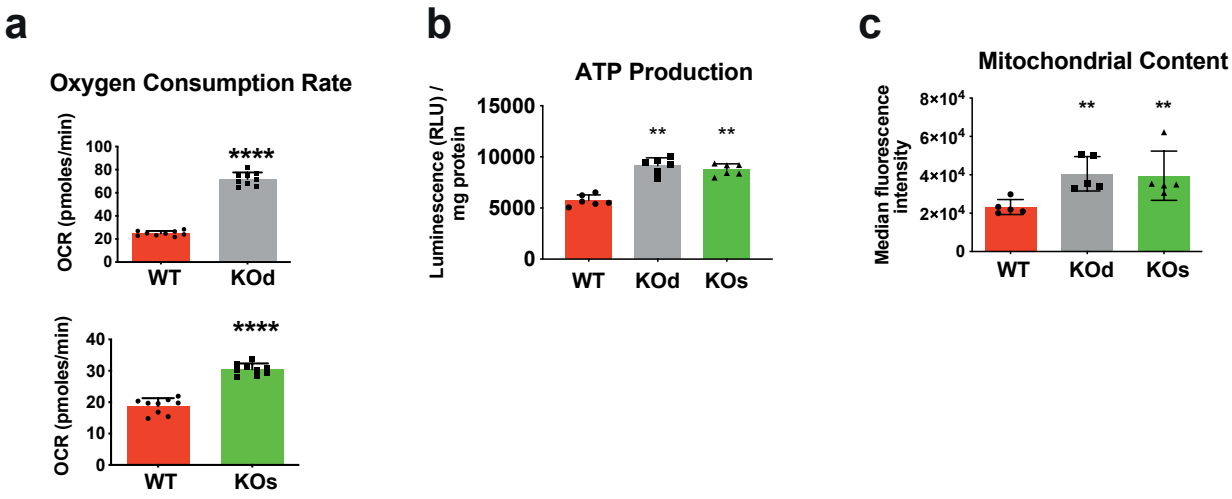

Appendix Figure S5. NNMT controls cancer cell metabolism by decreasing OXPHOS.
a-c: Bar plots quantification of basal oxygen consumption rates (n = 9, 3 experimental replicates, 3 technical replicates), ATP levels (n = 6, 3 experimental replicates, 2 technical replicates), and mitochondrial content (n = 5 experimental replicates) in SUM159PT KOd and KOs compared to WT cells. **P < 0.01, ****P < 0.0001; Mann-Whitney U-test. Data are mean ± SD.

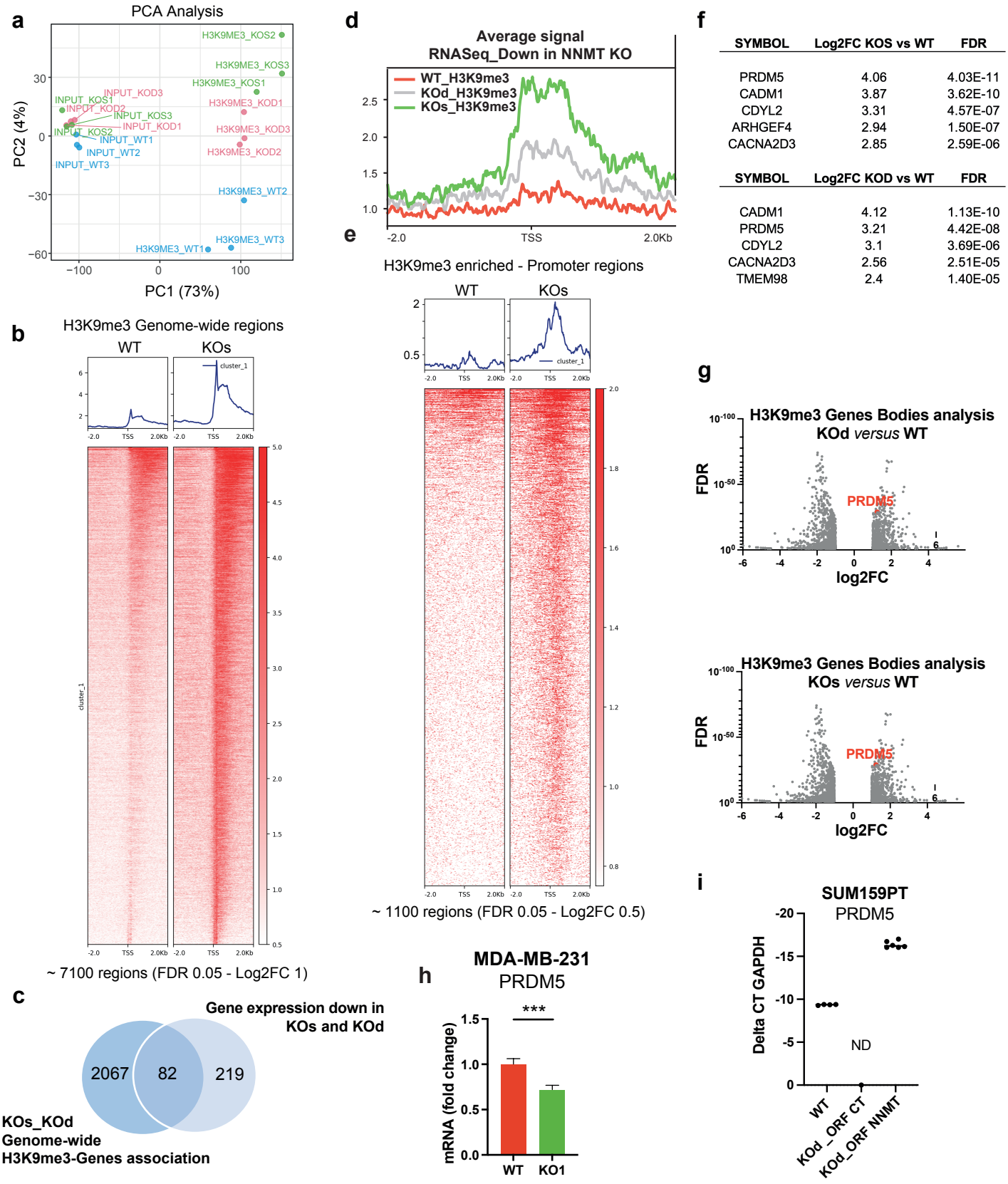

Appendix Figure 6. H3K9me3 ChIP-Seq analysis.

a, PCA plot depicting SUM159PT, KOs NNMT and KOd NNMT ChIP and Input samples.

b, H3K9me3 occupancy at peaks significantly enriched genome-wide in KOs condition versus WT (Log2FC 1, FDR > 0.05) assessed by ChIP-sequencing.

c, Venn diagram showing overlap between genes down-regulated upon NNMT knock-out and gene associated to H3K9me3 peak genome-wide in NNMT KOs and KOd cells in comparisons to WT. Peak-gene association was performed using GREAT software (Basal plus extension – settings: 5kb, 1kb, 50kb). 28% of the NNMT down-regulated genes are associated to H3K9me3 peaks.

d, H3K9me3 signal plot profile at TSS of the 301 genes significantly downregulated upon NNMT KO identified by mRNA-sequencing (cut-off: adjusted P < 0.05) assessed by ChIP-sequencing of SUM159PT WT, KOs, and KOd cells.

e, H3K9me3 occupancy at TSS in SUM159PT KOs versus WT contrast (Log2FC 0.5, FDR > 0.05) assessed by ChIP-sequencing.

f, Tables depicting Top 5 H3K9me3 hypermethylated gene within the promoter for both KOs versus WT and KOd versus WT comparisons. Log2Fc and FDR are shown.

g, Volcano plots depicting H3K9me3 peaks (cut-off: Log2FC 1, FDR < 0.1) detected within gene bodies, for both KOs versus WT and KOd versus WT comparisons. PRDM5 is highlighted in red.

h, Bar graph representing average PRDM5 mRNA expression in MDA-MB-231 WT and KO1 cells. n = 3 experimental replicates with 2 technical replicates each. ***P < 0.001; Mann-Whitney U-test. All data are means ± SD.

i, Bar graph representing PRDM5 mRNA expression using Delta CT (GAPDH), in SUM159PT WT, KOs_ORF CT and KOs_ORF NNMT (rescue NNMT). Data were depicted as Delta CT as PRDM5 was undetected in SUM159 KOs_ORF CT sample. n = 2 to 3 experimental replicates.

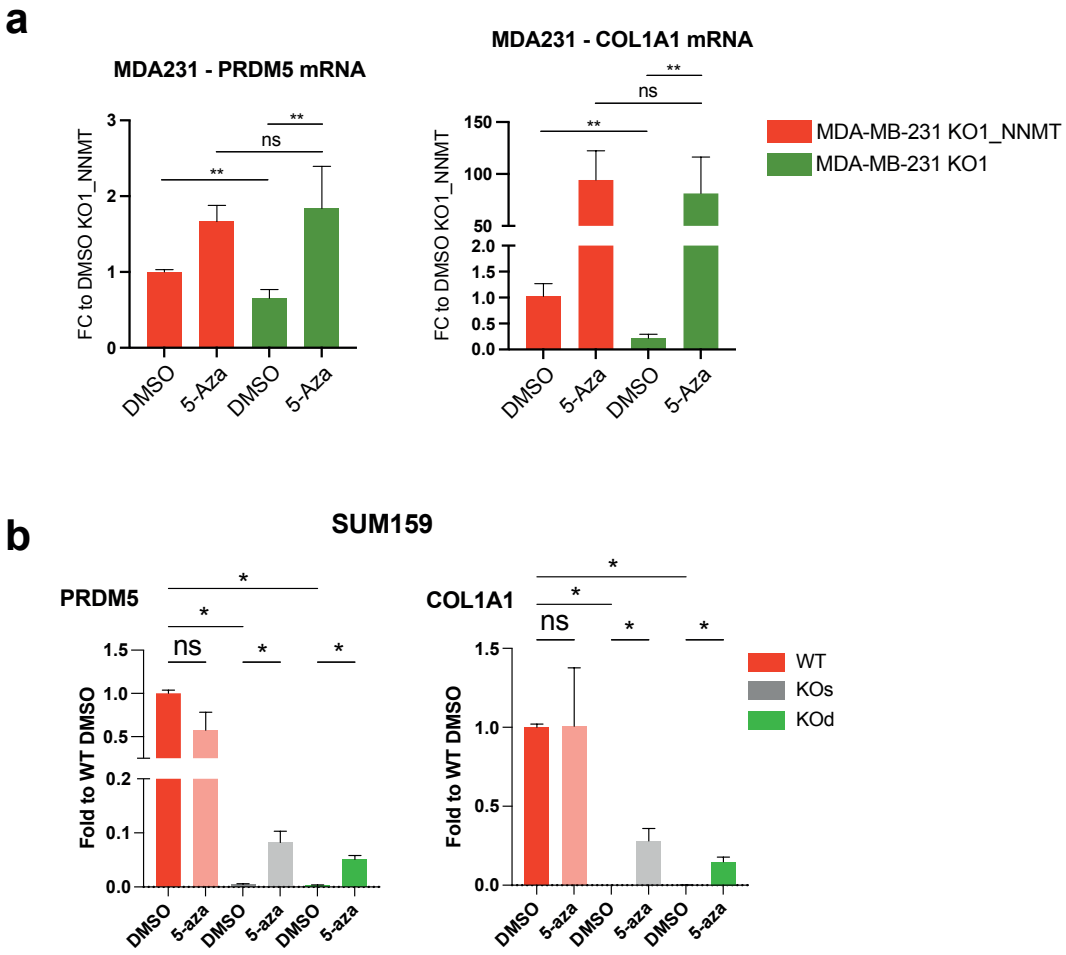

Appendix Figure S7. DNA methylation represses COL1A1 and PRDM5 expression upon NNMT ablation.

a, Bar graphs representing PRDM5 and COL1A1 mRNA expression upon 5- aza treatment (2 uM for 6 days) in MDA-MB-231 KO1_NNMT and KO1_RFP cells. n = 3 replicates. **P < 0.01, n.s., not significant; Mann-Whitney U-test. Data are means ± SD.

b, Bar graphs representing PRDM5 and COL1A1 mRNA expression two weeks after 5-aza removal from the medium, in NNMT WT, Kos, and KOd SUM159PT cells (n = 4 experimental replicates). *P < 0.05, **P < 0.01, ns., not significant; Mann-Whitney U-test. All data are means ± SEM.

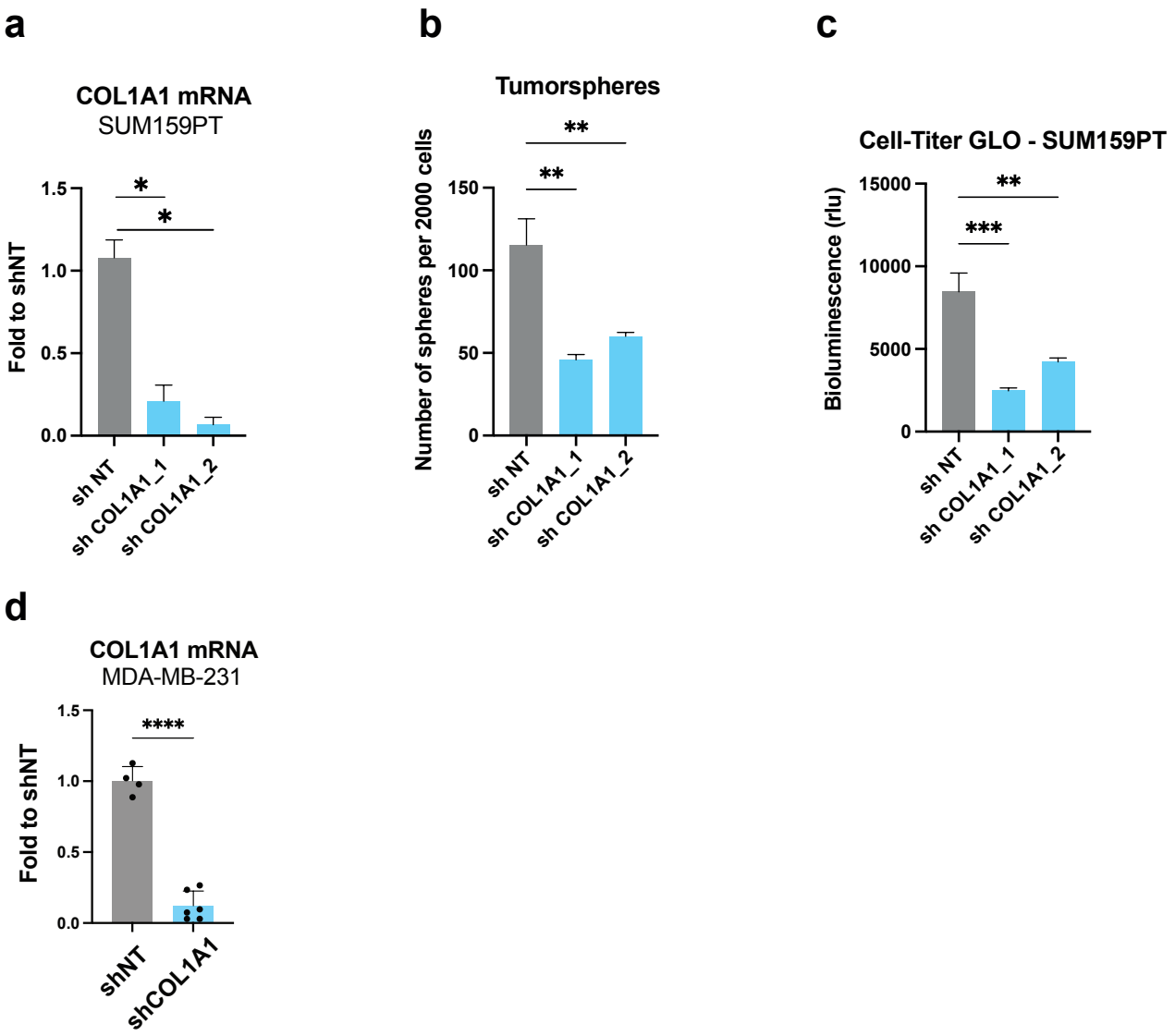

Appendix Figure S8. COL1A1 ablation decreases tumorsphere formation.

a, Bar graph representing COL1A1 expression in SUM159PT cells expressing sh NT or sh1 and sh2 targeting COL1A1. n = 2 experimental replicates with 2 technical replicates. *P < 0.05; Mann-Whitney U-test. All data are means ± SD.

b, Bar graph representing tumorspheres count per 2000 cells seeded in suspension in SUM159PT cells expressing sh NT, sh1 and sh2 targeting COL1A1. n = 4 experimental replicates. **P < 0.01; One-way ANOVA. All data are means ± SD.

c, Bar graph representing Cell-Titer GLO assay from tumorspheres grown SUM159PT cells expressing sh NT, sh1 and sh2 targeting COL1A1. n = 6 experimental replicates. **P < 0.01, ***P < 0.001; One-way ANOVA. All data are means ± SD.

d, Bar graph representing COL1A1 expression in MDA-MB-231 cells expressing sh NT or sh COL1A1. n = 4 replicates. ****P < 0.0001; Mann-Whitney U-test. All data are means ± SD.